

# Convective heat transport in stratified atmospheres at low and high Mach number

Evan H. Anders and Benjamin P. Brown

*Department of Astrophysical & Planetary Sciences, University of Colorado – Boulder and  
Laboratory for Atmospheric and Space Physics, Boulder, CO*

We study stratified convection in the context of plane-parallel, polytropically stratified atmospheres. We perform a suite of 2D and 3D simulations in which we vary the initial superadiabaticity ( $\epsilon$ ) and the Rayleigh number (Ra) while fixing the initial density stratification, aspect ratio, and Prandtl number. The evolved heat transport, quantified by the Nusselt number (Nu), follows scaling relationships similar to those found in the well-studied, incompressible Rayleigh-Bénard problem in both 2D and 3D and is not appreciably affected by the magnitude of  $\epsilon$ . The evolved Mach number (Ma) scales according to  $\text{Ma} \propto \epsilon^{1/2} \text{Ra}^\alpha$ , where  $\alpha = 0$  in 3D and  $\alpha \approx 1/4$  in 2D. At large values of  $\epsilon$ , significant density inversions appear in the evolved atmospheres and seem to persist in both 2D and 3D.

## INTRODUCTION

Convection transports energy in stellar and planetary atmospheres. In these objects, flows are compressible and feel the atmospheric stratification. While in some systems this stratification is negligible, it is significant in regions such as the convective envelope of the Sun, which spans 14 density scale heights. In the bulk of these systems, especially in the deep interior far below the surface, flows are at very low Mach number (Ma). Unfortunately, numerical constraints have restricted most studies of compressible convection to high Ma. These prior studies [1–6] have provided insight into the nature of convection in the low temperature, high Ma region near the Sun’s surface. Few fundamental properties of low Ma compressible convection, such as the scaling of convective heat transport, are known.

In the widely-studied Rayleigh-Bénard (RB) problem of incompressible Boussinesq convection, a negative temperature gradient causes convective instability. In the evolved solution, upflows and downflows are symmetrical, the temperature in the interior becomes isothermal, and the conductive flux ( $\propto \nabla T$ ) approaches zero there. For compressible convection in a stratified atmosphere, a negative entropy gradient causes convective instability. Early numerical experiments of moderate-to-high Ma compressible convection in two [1, 2, 5, 6] and three [3, 4, 7] dimensions revealed a different evolved state from the RB case. Downflow lanes become fast and narrow, and upflow lanes turn into broad, slow upwellings. Furthermore, the *entropy* gradient is negated by convection in the interior, so a significant temperature gradient and conductive flux can persist despite efficient convection.

In RB convection, there exist two primary dynamical control parameters: the Rayleigh number (Ra, the ratio of buoyant driving to diffusive damping) and the Prandtl number (Pr, the ratio of viscous to thermal diffusivity). These numbers control two useful measures of turbulence in the evolved solution: the Reynolds number (Re, the strength of advection to viscous diffusion) and the Peclet number (Pe, advection vs. thermal diffusion). In strati-

fied atmospheres, the magnitude of the unstable entropy gradient joins Ra and Pr as an important control parameter. This *superadiabatic excess* [5],  $\epsilon$ , sets the scale of the atmospheric entropy gradient. We find here that  $\epsilon$  primarily controls the Ma of the evolved solution.

In this letter we study the behavior of convective heat transport, quantified by the Nusselt number (Nu), in plane-parallel, two- and three-dimensional, polytropically stratified atmospheres. We vary  $\epsilon$  and Ra while holding Pr, aspect ratio, boundary conditions, and initial atmospheric stratification constant. We also examine the behavior of flow properties, as quantified by Ma and Re. We find here that the scaling of Nu in stratified, compressible convection is similar to that in Rayleigh-Bénard convection, and that this scaling is not appreciably changed by the magnitude of the superadiabaticity.

## EXPERIMENT

We examine a monatomic ideal gas with an adiabatic index of  $\gamma = 5/3$  whose equation of state is  $P = R\rho T$ . This is consistent with the approach used in earlier work [1–7] and is the simplest stratified extension of RB. We study atmospheres which are initially polytropically stratified,

$$\begin{aligned}\rho_0(z) &= \rho_t(1 + L_z - z)^m, \\ T_0(z) &= T_t(1 + L_z - z),\end{aligned}\quad (1)$$

where  $m$  is the polytropic index and  $L_z$  is the depth of the atmosphere. The polytropic index is set by the superadiabatic excess,  $\epsilon = m_{ad} - m$ , where  $m_{ad} = (\gamma - 1)^{-1}$  is the adiabatic value of  $m$ . The height coordinate,  $z$ , increases upwards in the range  $[0, L_z]$ . Subscript 0 indicates initial conditions and subscript  $t$  indicates values at  $z = L_z$ . We specify the depth of the atmosphere,  $L_z = e^{n_\rho/m} - 1$ , by choosing the number of density scale heights,  $n_\rho$ , it spans initially. Throughout this letter we set  $n_\rho = 3$ . Satisfying hydrostatic equilibrium sets the value of gravity,  $g = RT_t(m + 1)$ , which is constant with depth. We study atmospheres with aspect ratios of 4 where both the

$x$  and  $y$  coordinates have the range  $[0, 4L_z]$ . In our 2D cases, we only consider  $x$  and  $z$ .

These domains are nondimensionalized by setting all thermodynamic variables to unity at  $z = L_z$ , choosing  $R = T_t = \rho_t = 1$ . By this choice, the non-dimensional length scale is the inverse temperature gradient scale and the timescale is the isothermal sound crossing time,  $\tau_I$ , of this unit length. Meaningful convective dynamics occur on timescales of the atmospheric buoyancy time,  $t_b = \tau_I \sqrt{L_z/g\epsilon}$ .

At fixed  $n_\rho$ , convective dynamics are controlled by  $\epsilon$  as well as the atmospheric diffusivities. At a fixed value of  $\epsilon$ , the diffusivities are set by the Rayleigh number (Ra) and the Prandtl number (Pr),

$$\text{Ra}_t = \frac{gL_z^3(\Delta S_0/c_P)}{\nu_t \chi_t}, \quad \text{Pr} = \frac{\nu}{\chi}, \quad (2)$$

where  $\Delta S_0 = \epsilon \ln(1 + L_z)$  is the initial entropy difference between the top and bottom boundaries,  $c_P = \gamma/(\gamma - 1)$  is the specific heat at constant pressure, and  $\nu$  and  $\chi$  are the thermal diffusivity and kinematic viscosity, respectively. Throughout this work we specify that  $\text{Pr} = 1$  and is depth invariant. Polytropes, as specified in (1), are in thermal equilibrium. Thus, the initial thermal conductivity,  $\kappa_0 = \chi \rho_0$ , is constant with depth. By these choices,  $\nu(z) \equiv \chi(z) \equiv \chi_t/\rho_0$ . This formulation sets Ra at the bottom of the domain greater than  $\text{Ra}_t$  by a factor of  $e^{2n_\rho}$ . Henceforth when we specify Ra we are referring to  $\text{Ra}_t$ . The full values of  $\kappa = \rho \chi$  and  $\mu = \rho \nu$  (the dynamic viscosity) are free to evolve as the density profile evolves.

Under this formulation, diffusivities scale as

$$\chi_t = \nu_t \propto \sqrt{\frac{\epsilon}{\text{Ra}_t}} \quad (3)$$

for constant  $\text{Pr} = 1$ , as in this work. We carry out two experiments in this letter: one in which we fix  $\epsilon$  and increase Ra, thus increasing the diffusive timescales, and a second in which we fix Ra and raise  $\epsilon$ , thus modifying the ratio of the diffusive timescales to the buoyant timescale.

We evolve the Fully Compressible Navier-Stokes equations,

$$\frac{\partial \ln \rho}{\partial t} + \nabla \cdot \mathbf{u} = -\mathbf{u} \cdot \nabla \ln \rho, \quad (4)$$

$$\frac{\partial \mathbf{u}}{\partial t} + \nabla T - \nu \nabla \cdot \bar{\boldsymbol{\sigma}} - \bar{\boldsymbol{\sigma}} \cdot \nabla \nu = -\mathbf{u} \cdot \nabla \mathbf{u} - T \nabla \ln \rho + \mathbf{g} + \nu \bar{\boldsymbol{\sigma}} \cdot \nabla \ln \rho, \quad (5)$$

$$\begin{aligned} \frac{\partial T}{\partial t} - \frac{1}{c_V} (\chi \nabla^2 T + \nabla T \cdot \nabla \chi) &= \\ &- \mathbf{u} \cdot \nabla T - (\gamma - 1) T \nabla \cdot \mathbf{u} \\ &+ \frac{1}{c_V} (\chi \nabla T \cdot \nabla \ln \rho + \nu [\bar{\boldsymbol{\sigma}} \cdot \nabla] \cdot \mathbf{u}), \end{aligned} \quad (6)$$

with the viscous stress tensor given by

$$\sigma_{ij} \equiv \left( \frac{\partial u_i}{\partial x_j} + \frac{\partial u_j}{\partial x_i} - \frac{2}{3} \delta_{ij} \nabla \cdot \mathbf{u} \right). \quad (7)$$

Taking an inner product of (5) with  $\rho \mathbf{u}$  and adding it to  $\rho c_V \times (6)$  reveals the full energy equation,

$$\frac{\partial}{\partial t} \left( \rho \left[ \frac{|\mathbf{u}|^2}{2} + c_V T + \phi \right] \right) + \nabla \cdot (\mathbf{F}_{\text{conv}} + \mathbf{F}_{\text{cond}}) = 0, \quad (8)$$

where  $\mathbf{F}_{\text{conv}} \equiv \mathbf{F}_{\text{enth}} + \mathbf{F}_{\text{KE}} + \mathbf{F}_{\text{PE}} + \mathbf{F}_{\text{visc}}$  is the convective flux and  $\mathbf{F}_{\text{cond}} = -\kappa \nabla T$  is the conductive flux. The individual contributions to  $\mathbf{F}_{\text{conv}}$  are the enthalpy flux,  $\mathbf{F}_{\text{enth}} \equiv \rho \mathbf{u} (c_V T + P/\rho)$ ; the kinetic energy flux,  $\mathbf{F}_{\text{KE}} \equiv \rho |\mathbf{u}|^2 \mathbf{u}/2$ ; the potential energy flux,  $\mathbf{F}_{\text{PE}} \equiv \rho \mathbf{u} \phi$  (with  $\phi \equiv -gz$ ); and the viscous flux,  $\mathbf{F}_{\text{visc}} \equiv -\rho \nu \mathbf{u} \cdot \bar{\boldsymbol{\sigma}}$ . Understanding how each of these fluxes interact is crucial in characterizing convective heat transport.

We utilize the Dedalus<sup>1</sup> [8] pseudospectral framework to time-evolve (4)-(6) using an implicit-explicit (IMEX), third-order, four-step Runge-Kutta timestepping scheme RK443 [9]. We decompose our thermodynamic variables such that  $T = T_0 + T_1$  and  $\ln \rho = (\ln \rho)_0 + (\ln \rho)_1$ , and the velocity is  $\mathbf{u} = u \hat{x} + v \hat{y} + w \hat{z}$ . In our 2D runs,  $v = 0$ . Subscript 0 variables, set by (1), have no time derivative and vary only in  $z$ . Variables are time-evolved on a dealiased Chebyshev (vertical) and Fourier (horizontal, periodic) domain in which the physical grid dimensions are 3/2 the size of the coefficient grid. Domain sizes range from 64x256 coefficients at the lowest values of Ra to 1024x4096 coefficients at Ra  $> 10^7$  in 2D, and from 64x128<sup>2</sup> to 256x512<sup>2</sup> in 3D. By using IMEX timestepping, we implicitly step the stiff linear acoustic wave contribution and are able to efficiently study flows at high ( $\sim 1$ ) and low ( $\sim 10^{-4}$ ) Ma. Our equations take the form of the FC equations in [10], extended to include  $\nu$  and  $\chi$  which vary with depth, and we follow the approach there. This IMEX approach has been successfully tested against a nonlinear benchmark of the compressible Kelvin-Helmholtz instability [11].

We impose impenetrable, stress free, fixed temperature boundary conditions at the top and bottom of the domain such that  $w = \partial_z u = T_1 = 0$  at  $z = \{0, L_z\}$ .  $T_1$  is initially filled with random white noise whose magnitude is infinitesimal compared to  $T_0$  and  $\epsilon$ . We filter this noise spectrum in coefficient space, such that only the lower 25% of the coefficients have power. All reported results are taken from time averages over many  $t_b$  beginning  $\{100, 40\}t_b$  after the start of our {2D, 3D} simulations in order to assure our results are not biased by the convective transient.

---

<sup>1</sup> <http://dedalus-project.org/>

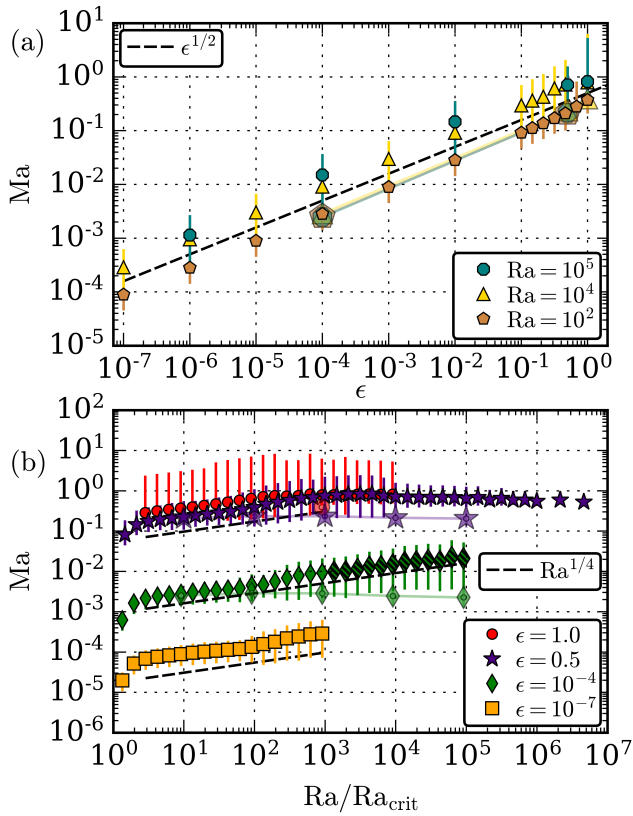


FIG. 1. The mean adiabatic Mach number of long-time-averaged profiles is shown. Error bars show the full range of Ma over the depth of the atmosphere. (a) Ma, at various values of Ra, is plotted as a function of  $\epsilon$ . (b) Ma, at various values of  $\epsilon$ , is plotted as a function of  $\text{Ra}/\text{Ra}_{\text{crit}}$ . Larger symbols with white dots designate 3D runs.

## RESULTS & DISCUSSION

Solutions were time-evolved until a long time average of the fluxes showed little variance with depth. A linear stability analysis determined that convective onset occurs at  $\text{Ra}_{\text{crit}} = \{11.15, 10.06, 10.97, 10.97\}$  for  $\epsilon = \{1.0, 0.5, 10^{-4}, 10^{-7}\}$ , respectively.

We measure the adiabatic Mach number ( $\text{Ma} = |\mathbf{u}|/\sqrt{\gamma T}$ ), and find that it is a strong function of  $\epsilon$  and a weak function of Ra. In our 2D runs, when  $\text{Ma} < 1$ , we observe a scaling law of  $\text{Ma}(\text{Ra}, \epsilon) \propto \epsilon^{1/2} \text{Ra}^{1/4}$ . This relation breaks down as the mean Ma approaches 1 (see Fig. 1). This transition occurs near  $\text{Ra}/\text{Ra}_{\text{crit}} \approx \{10^2, 10^3\}$  for  $\epsilon = \{1, 0.5\}$ . We conjecture that the scaling of Ma with Ra is due to high-velocity “spinners” which form between upflow and downflow lanes in 2D, and which are constantly fed by the relatively stationary upflows and downflows (BEN NEED CITES). In our limited 3D runs, Ma appears to be a function of  $\epsilon$  alone, with  $\text{Ma} \propto \epsilon^{1/2}$ , so at high Ra,  $\text{Ma}_{3D} < \text{Ma}_{2D}$ . Simulations in the range of  $\text{Ra}/\text{Ra}_{\text{crit}} > 10^3$  at  $\epsilon = 10^{-4}$  exhibited “windy” states

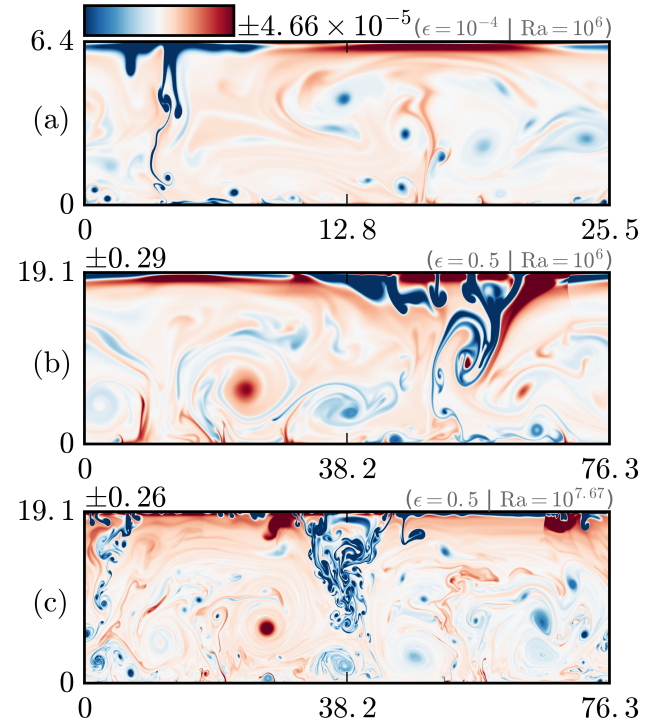


FIG. 2. Characteristic entropy fluctuations in evolved 2D flows roughly  $140t_b$  after the start of simulations. The time- and horizontally-averaged profile is removed in all cases. (a) A low Ma flow at moderate Ra. (b) A high Ma flow at the same Ra as in (a). (c) A high Ma flow at high Ra. Shock systems can be seen in the upper atmosphere of the high Ma flows, for example at  $(x, z) \sim (70, 15 - 19)$  in (b) and  $(x, z) \sim (65, 17 - 19)$  in (c).

of convection, in which a large-scale horizontal shearing flow replaced the more standard upflow/downflow morphology of convection, similar to analogous states which have been studied in RB convection [12]. These states are represented in Figs. 1, 3, & 4 as hatched points, and while this phenomenon does not appear to greatly modify the scaling of fluid properties measured in this work, these states warrant further investigation.

Low Ma flows (e.g.,  $\epsilon = 10^{-4}$ ) display the classic narrow downflow and broad upflow lanes of stratified convection (Fig. 2a). At high Ma (e.g.,  $\epsilon = 0.5$ ,  $\text{Ra}/\text{Ra}_{\text{crit}} \gtrsim 10^3$ ), bulk thermodynamic structures are similar but shock systems form in the upper atmosphere near downflow lanes (Fig. 2b&c). These shock phenomena were reported in two [2] and three [13] dimensional polytropic simulations previously. As in (3), diffusivities become small as Ra is increased to large values (Fig. 2c) and thermodynamic structures break up into small eddies which traverse the domain repeatedly before diffusing. Furthermore, the value of  $\epsilon$  sets the size of the evolved thermodynamic fluctuations from their adiabatic values, as evidenced by the scalings of the colorbars.

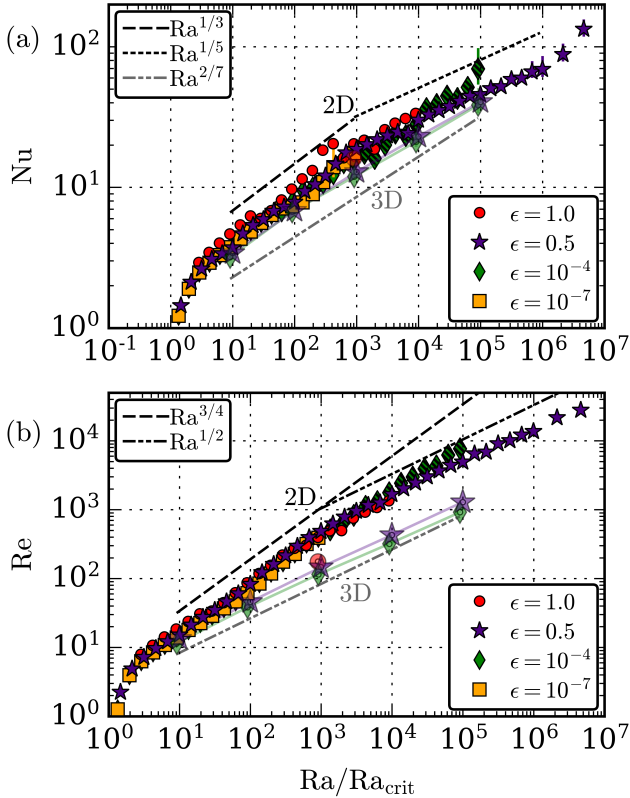


FIG. 3. Flow properties at high and low  $\epsilon$ . (a)  $\text{Nu}$  vs.  $\text{Ra}/\text{Ra}_{\text{crit}}$ . Errors bars indicate the variance of  $\text{Nu}$  with depth; large error bars indicate a poorly converged solution. (b)  $\text{Re}$  vs.  $\text{Ra}/\text{Ra}_{\text{crit}}$ .  $\text{Re}$  is measured at the midplane of the atmosphere. Larger symbols with white dots designate 3D runs.

The efficiency of convection is quantified by the Nusselt number ( $\text{Nu}$ ).  $\text{Nu}$  is well-defined in RB convection as the total flux normalized by the steady-state conductive flux [14, 15]. In stratified convection  $\text{Nu}$  is more difficult to define, and we use a modified version of a traditional stratified Nusselt number [1, 5],

$$\text{Nu} \equiv \frac{\langle F_{\text{conv},z} + F_{\text{cond},z} - F_A \rangle}{\langle F_{\text{cond},z} - F_A \rangle} = 1 + \frac{\langle F_{\text{conv},z} \rangle}{\langle F_{\text{cond},z} - F_A \rangle} \quad (9)$$

where  $F_{\text{conv},z}$  and  $F_{\text{cond},z}$  are the z-components of  $\mathbf{F}_{\text{conv}}$  and  $\mathbf{F}_{\text{cond}}$ , and  $\langle \rangle$  are volume averages.  $F_A \equiv -\langle \kappa \rangle \partial_z T_{\text{ad}}$  is the conductive flux of the proper corresponding adiabatic atmosphere. For a compressible, ideal gas in hydrostatic equilibrium,  $\partial_z T_{\text{ad}} \equiv -g/c_P$  [16]. It is important to measure the evolved value of  $\langle \kappa \rangle = \langle \rho \chi \rangle$ , which is nearly  $\kappa_0$  for small  $\epsilon$  but changes appreciably for large values of  $\epsilon$ . In incompressible Boussinesq convection, where  $\nabla S = 0$  only when  $\nabla T = 0$ , this definition reduces to the traditionally defined Nusselt number [14, 15].

The variation of  $\text{Nu}$  with  $\text{Ra}$  is shown in Fig. 3a. We find that the  $\text{Nu}$  depends primarily on  $\text{Ra}$ , not on  $\epsilon$ , except where dynamical regimes change. In 2D and at low

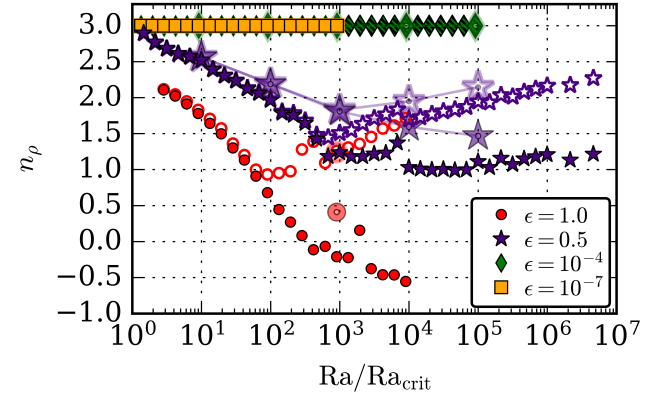


FIG. 4. Solid symbols show the density contrast measured in density scale heights between the upper and lower boundary,  $n_\rho = \ln[\rho(z = 0)/\rho(z = L_z)]$ . Empty symbols show  $n_\rho = \ln[\max(\rho)/\min(\rho)]$ . At low  $\epsilon$  the evolved  $n_\rho$  is close to the initial conditions of  $n_\rho = 3$ . At high  $\epsilon$ , the density stratification decreases. Once the mean Ma approaches 1 (at  $\text{Ra}/\text{Ra}_{\text{crit}} \approx \{10^2, 10^3\}$  for  $\epsilon = \{1, 0.5\}$  as in Fig. 1b), density inversions form within the thermal boundary layers. Larger symbols represent 3D runs.

to moderate  $\text{Ra}$ ,  $\text{Nu} \propto \text{Ra}^{1/3}$  regardless of  $\epsilon$ , reminiscent of scaling laws in Rayleigh-Bénard boundary layer theory [17–19]. As the flow becomes supersonic,  $\text{Nu} \propto \text{Ra}^{1/5}$ . It is also important to note that the value of  $\text{Nu}$  is heavily dependent upon the specific thermodynamic structures of the solution, as double roll states will transport heat more efficiently than single roll states, and slight changes in  $\text{Ra}$  can result in a simulation latching on to one solution or the other. Select simulations were run at aspect ratios of 8 and 16, and identical flow morphologies were obtained, which suggests that these states are sensitive to parameters other than the width of the domain. In our limited 3D runs, it appears that  $\text{Nu} \propto \text{Ra}^{2/7}$ , a classic scaling law seen in RB studies [14].

The rms Reynolds number ( $\text{Re} = |\mathbf{u}|L_z/\nu$ ) and Peclet number ( $\text{Pe} = \text{Pr} \text{Re}$ ) compare the importance of advection to diffusion in the evolved convective state. For  $\text{Pr} = 1$ , such as in this work,  $\text{Pe} = \text{Re}$ . Our choice of  $\{\nu, \chi\} \propto \rho_0^{-1}$  drastically changes the value of  $\text{Re}$  between the top and bottom of the atmosphere. We report values of  $\text{Re}$  at the midplane ( $z = L_z/2$ ) of the atmosphere in Fig. 3b. Largely we find that  $\text{Re}$  depends on  $\text{Ra}$ , but not  $\epsilon$ , except when the flow states change. In 2D and at low  $\text{Ra}$ ,  $\text{Re} \propto \text{Ra}^{3/4}$ . The heightened scaling of  $\text{Re}$  in 2D is due to the scaling of velocity (Ma) with  $\text{Ra}$ , as is seen in Fig. 1. When the flows become supersonic, this scaling gives way to  $\text{Re} \propto \text{Ra}^{1/2}$ , as expected by the scaling of diffusivities in (3). In our limited 3D runs, the scaling of  $\text{Re}$  is  $\text{Re} \propto \text{Ra}^{1/2}$ , consistent with the supersonic results.

In the evolved state, the flows change the density stratification, as shown in Fig. 4. Here we take two different measurements of the stratification present in the time-

averaged, horizontally-averaged density profile: the density difference between the max and min value of the density profile (empty symbols) and the density difference between the top and bottom of the atmosphere (solid symbols). We find that supersonic flows support persistent density inversions (empty symbols) in the boundary layers, as was reported by [4]. We find this in 2D and 3D, even at very large  $\epsilon$ . Surprisingly, the evolved  $n_\rho$  is always less than the initial  $n_\rho = 3$ , and turbulent pressure support plays a larger role than atmospheric slumping. The agreement of Nu & Re across  $\epsilon$  (Fig. 3), particularly at low Ra in which all four of our cases collapse onto a single power law, is striking in light of the vastly different evolved stratifications felt by the flows.

In summary, we have found that the evolved flow properties of stratified, compressible convection scale in a manner reminiscent of RB convection. We argue that polytropically stratified atmospheres are the natural extension of the RB problem with an additional control parameter,  $\epsilon$ , whose primary role is to set the Ma of the flows. We show that other properties of the evolved solutions (Nu, Re) are nearly identical at vastly different values of  $\epsilon$ , except for where there is a transition between the subsonic and supersonic regimes. We also see that Nu scales similarly in 3D and 2D, and that Ma in 3D solutions seems to be a function of  $\epsilon$  alone, allowing for simple specification of the evolved Ma using input parameters.

The stratification of these polytropic atmospheres evolves in a complex manner. Future work should aim to understand the importance of stratification on convective heat transport and other flow properties.

Our studies here will serve as a foundation for comparing heat transport in stratified convection to that in RB convection [14] and for better quantifying transport in stratified convection. These results can be used to determine if fluid properties scale appropriately in simplified equation sets, such as the anelastic equations. This work will also be useful in coming to understand more realistic systems, such as rapidly rotating atmospheres [20], atmospheres bounded by stable regions [21], and regions with realistic profiles of  $\kappa$ .

### acknowledgements

EHA acknowledges the support of the University of Colorado's George Ellery Hale Graduate Student Fellowship. This work was additionally supported by NASA LWS grant number NNX16AC92G. Computations were conducted with support by the NASA High End Computing (HEC) Program through the NASA Advanced Su-

percomputing (NAS) Division at Ames Research Center on Pleiades with allocations GID s1647 and GID g26133. We thank Jon Aurnou, Axel Brandenburg, Keith Julien, Mark Rast, and Jeff Oishi for many useful discussions. We also thank the two anonymous referees whose careful comments greatly improved the quality of this letter.

- 
- [1] N. E. Hurlburt, J. Toomre, and J. M. Massaguer, *Astrophys. J.* **282**, 557 (1984).
  - [2] F. Cattaneo, N. E. Hurlburt, and J. Toomre, *ApJL* **349**, L63 (1990).
  - [3] N. H. Brummell, N. E. Hurlburt, and J. Toomre, *Astrophys. J.* **473**, 494 (1996).
  - [4] A. Brandenburg, K. L. Chan, Å. Nordlund, and R. F. Stein, *Astronomische Nachrichten* **326**, 681 (2005), astro-ph/0508404.
  - [5] E. Graham, *Journal of Fluid Mechanics* **70**, 689 (1975).
  - [6] K. L. Chan, S. Sofia, and C. L. Wolff, *Astrophys. J.* **263**, 935 (1982).
  - [7] F. Cattaneo, N. H. Brummell, J. Toomre, A. Malagoli, and N. E. Hurlburt, *Astrophys. J.* **370**, 282 (1991).
  - [8] K. Burns, G. Vasil, J. Oishi, D. Lecoanet, and B. Brown, *Dedalus: Flexible framework for spectrally solving differential equations*, Astrophysics Source Code Library (2016), 1603.015.
  - [9] U. M. Ascher, S. J. Ruuth, and R. J. Spiteri, *Applied Numerical Mathematics* **25**, 151 (1997).
  - [10] D. Lecoanet, B. P. Brown, E. G. Zweibel, K. J. Burns, J. S. Oishi, and G. M. Vasil, *Ap. J.* **797**, 94 (2014), 1410.5424.
  - [11] D. Lecoanet, M. McCourt, E. Quataert, K. J. Burns, G. M. Vasil, J. S. Oishi, B. P. Brown, J. M. Stone, and R. M. O'Leary, *MNRAS* **455**, 4274 (2016), 1509.03630.
  - [12] D. Goluskin, H. Johnston, G. R. Flierl, and E. A. Spiegel, *Journal of Fluid Mechanics* **759**, 360 (2014).
  - [13] A. Malagoli, F. Cattaneo, and N. H. Brummell, *ApJL* **361**, L33 (1990).
  - [14] H. Johnston and C. R. Doering, *Physical Review Letters* **102**, 064501 (2009), 0811.0401.
  - [15] J. Otero, R. W. Wittenberg, R. A. Worthing, and C. R. Doering, *Journal of Fluid Mechanics* **473**, 191 (2002).
  - [16] E. A. Spiegel and G. Veronis, *Astrophys. J.* **131**, 442 (1960).
  - [17] S. Grossmann and D. Lohse, *Journal of Fluid Mechanics* **407**, 27 (2000).
  - [18] G. Ahlers, S. Grossmann, and D. Lohse, *Rev. Mod. Phys.* **81**, 503 (2009).
  - [19] E. M. King, S. Stellmach, and J. M. Aurnou, *Journal of Fluid Mechanics* **691**, 568 (2012).
  - [20] K. Julien, E. Knobloch, A. M. Rubio, and G. M. Vasil, *Physical Review Letters* **109**, 254503 (2012).
  - [21] N. E. Hurlburt, J. Toomre, and J. M. Massaguer, *Astrophys. J.* **311**, 563 (1986).